Textile Multilayer Cavity Slot Monopole For UHF Applications

Sree Pramod Pinapati, *Student Member, IEEE*, Damith Chinthana Ranasinghe, *Member, IEEE*, and Christophe Fumeaux, *Senior Member, IEEE*

***Abstract*—A low-profile multilayer textile antenna inspired by a folded cavity with a broad slot monopole is presented for wearable applications in the UHF band. The proposed geometry has total dimensions of $0.34\lambda_0 \times 0.22\lambda_0 \times 0.0149\lambda_0$ at a targeted resonance frequency of 923 MHz and achieves a fractional bandwidth of 3.0% on-body. The antenna is fed by a flexible shielded stripline to enhance wearability, and a substantial overall size reduction is achieved through a combination of miniaturization techniques amenable for textile implementation. A systematic design procedure along with a simple fabrication process including the use of computerized embroidery is a salient feature of the proposed geometry. Good agreement between simulation and measurement results in various conditions validates the proposed structure.**

***Index Terms*—Broad-slot, embroidery, slot monopole, UHF antennas, wearable antennas.**

I. Introduction

WEARABLE antennas have attracted increasing attention in the last decade for use in healthcare and security applications [1]. This has fostered significant development in antenna topologies suitable for wearable applications, such as dipoles [2], cavity-backed slots [3], patches [4], or planar inverted-F antenna [5]. Unidirectional radiation is generally preferred to minimize energy coupling into the body. Consequently, antennas including ground planes are naturally suitable, with cavity-backed slots being particularly attractive due to their variety of feeding mechanisms [3], [6]. Favorable regulations in the global UHF Industrial, Scientific, and Medical (ISM) bands (865–928 MHz) offer an attractive choice for many wearable applications as this can provide the possibility for passive operation [7], [8]. However, at UHF frequencies, antenna size becomes an issue, in particular for cavity-backed slot antennas where the typically planar dimensions are in the order of $0.5\lambda_g \times 0.5\lambda_g$. While the size can be reduced, this occurs at the expense of a narrower bandwidth. In this letter, a compact low-profile textile cavity-backed slot antenna capable of operating across the widest UHF ISM band (with bandwidth of 26 MHz) is presented for wearable applications in which the total size of the antenna is $0.34\lambda_0 \times 0.22\lambda_0 \times 0.02\lambda_0$. The main contributions of this work are the systematic integration of multiple miniaturization techniques to realize a compact electrically thin cavity-backed slot antenna incorporating a ground plane and a textile feed. This combination of features makes the antenna suitable for wearable applications at the UHF band with a relatively large bandwidth for the compact size compared to a standard cavity-backed slot antenna without any miniaturization techniques.

This letter is organized as follows: Design specifications and the proposed geometry are provided in Section II; the specific design steps are detailed in Section III; fabrication details and measurements are discussed in Section IV; comparisons to open literature are covered in Section V; and concluding remarks are provided in Section VI.

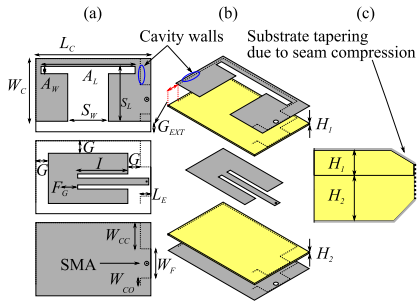

Fig. 1. Geometry of the proposed antenna. The optimized parameters are $G_{EXT} = 10$ mm, $W_C = 60$ mm, $L_C = 100$ mm, $L_E = 10$ mm, $S_L = 52.5$ mm, $S_W = 39$ mm, $A_L = 90$ mm, $A_W = 7$ mm, $W_F = 28$ mm, $W_{CO} = 7$ mm, $W_{CC} = 25$ mm, $G = 12$ mm, $I = 43$ mm, $F_G = 1$ mm, $H_1 = 1.6$ mm, $H_2 = 3.2$ mm. Shaded gray areas represent metallization layers and dotted lines represent embroidered conducting walls. From left to right: (a) 2-D layered view, (b) 3-D exploded view, (c) cross-sectional view of seam compression at the cavity walls.

II. Design Specifications and Proposed Geometry

For wearable applications, the antenna must be low-profile, flexible, unobtrusive, and preferably have a textile feed. Electrically, the antenna is specified to operate at a target resonance frequency of 923 MHz—the center frequency of the Australian UHF RFID band. For generality and scalability of the design, we target a 10-dB impedance bandwidth of 3.0% on-body to comply with the broadest UHF band exemplified by the North American band with a fractional bandwidth of 2.8%.

To satisfy the above-mentioned requirements, a geometry derived from a folded cavity with a slot-monopole antenna fed by a shielded stripline has been selected. A schematic view of the proposed multilayer structure is shown in Fig. 1. The top layer contains a broad slot monopole as a radiating element, the middle layer accommodates the feeding mechanism, and the bottom layer is the finite ground plane. Computerized

Manuscript received June 3, 2017; accepted July 20, 2017. Date of publication August 3, 2017; date of current version August 28, 2017. This work was supported by the Australia Research Council under Discovery Project DP160103039. *(Corresponding author: Sree Pramod Pinapati.)*

The authors are with the School of Electrical and Electronic Engineering, University of Adelaide, Adelaide, SA 5005, Australia (e-mail: sree.pinapati@adelaide.edu.au; damith.ranasinghe@adelaide.edu.au; christophe.fumeaux@adelaide.edu.au).

Color versions of one or more of the figures in this letter are available online at http://ieeexplore.ieee.org.

Digital Object Identifier 10.1109/LAWP.2017.2731978

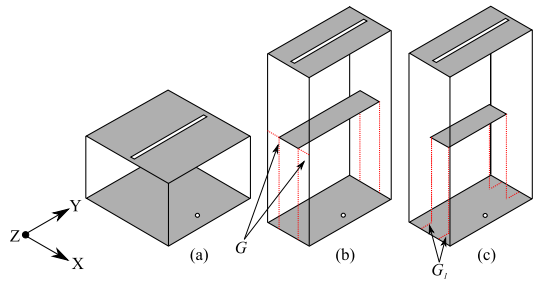

Fig. 2. (a) Standard cavity-backed slot antenna. (b) Miniaturized step 1. (c) Miniaturized step 2.

embroidery with conducting threads around the sides of the antenna provides a semiclosed cavity structure.

III. Design

To satisfy the requirements of flexibility, the antenna substrate is selected as Cumming Microwave PF-4, a highly flexible low-loss foam with a relative permittivity of 1.06 and a dielectric loss tangent of $\delta = 0.0001$. The metallization layers are created using Marktex NCS95R-CR metallized textile with an empirically determined sheet resistance of 0.09 $\Omega/\square$ over the desired frequency range.

A. Folded Cavity

A conventional cavity-backed slot antenna has dimensions of approximately $0.5\lambda_g \times 0.5\lambda_g$ for the cavity and a slot length of $0.5\lambda_g$, where λ_g is the guide wavelength as shown in Fig. 2(a). To reduce one of the dimensions, folding operations can be performed that would naturally reduce one of the dimensions from $0.5\lambda_g$ to $0.25\lambda_g$ while leaving the other dimension unchanged [9], [10]. In the current geometry, the antenna is shortened along the *x*-axis, leading to the geometry in Fig. 2(b), where the two edges parallel to the slot on either side are folded and joined at the back of the antenna. Relative to the standard geometry, the folded geometry is doubled in thickness and has a middle metallic layer that is separated from the cavity walls in the *x*-direction by a gap G [see Fig. 2(b)]. This gap G can be seen as increasing the capacitive loading on the slot due to the field confinement in the gap. To obtain further miniaturization, the same idea of capacitive loading can be extended to the *y*-axis [see Fig. 2(c)]. Specifically, by shrinking the middle layer by an additional G_1 along the *y*-axis, a larger reduction in resonance frequency is obtained. By this stage, the antenna is strictly speaking no longer "folded." For convenience, G_1 is chosen to be the same as G.

To further reduce the overall size, the top substrate is made thinner as this increases the capacitive loading on the slot. Consequently, the antenna becomes vertically asymmetric with $H_1 < H_2$. As the substrate material comes in specified thicknesses, the top and bottom substrates are set as $H_1 = 1.6$ mm and $H_2 = 3.2$ mm, respectively. With the above-mentioned steps, the antenna resonance frequency is reduced by 16% for the antenna in Fig. 2(c) if retaining the same overall planar dimensions as in Fig. 2(b).

B. Slot Modifications

Further size reductions can be achieved by: 1) changing the slot to an H-shaped slot; 2) making a slot monopole.

The H-shaped modification achieves miniaturization by extending the current path length, in which case the critical parameter is A_L, where an optimal choice can further reduce the resonance frequency by nearly 30%. Observing now that a slot antenna in its fundamental mode has a magnetic wall symmetry in its center, a sizeable reduction can be achieved by cutting the antenna in half to create a slot monopole [11].

To scale the resonance frequency back to the target of 923 MHz after all the miniaturization steps, the main parameters to optimize are the width of the cavity and slot length (W_C and S_L). Bandwidth increase is obtained by optimizing the slot width S_W as this defines the aperture where fields can escape the antenna. Alternatively, increasing the gap size G increases the bandwidth—as tradeoff to miniaturization—as an increased gap size contributes less capacitance.

Performing these modifications, the antenna size can be reduced to $0.31\lambda_0 \times 0.19\lambda_0$ or in absolute terms 60×100 mm^2 with a fractional bandwidth of 3.8%. It is noted that these are not the final dimensions of the antenna due to the changes described in Sections III-C–III-E. The achieved bandwidth is for a thickness of $0.0149\lambda_0$, noting that a standard cavity-backed slot at the same thickness would exhibit a bandwidth of 1.5%, showing that the current topology is significant improvement over a standard design.

C. Textile Feed

The examination of the field plots in the cavity reveals that the electric fields at the fundamental resonance are in opposite directions in the top and bottom substrates of the cavity. This, combined with the presence of a metallic middle layer, suggests that a shielded stripline feeding mechanism shown in Fig. 1(b) is a highly suitable option. Impedance matching is facilitated by varying the inset position I.

D. Seam Compression

Embroidered structures exhibit a compression of the substrate at the seams, as illustrated in Fig. 1(c), where it can be observed that the top and bottom metallized textile planes become tapered. This alters the fields in the cavity [3], consequently the antenna needs to be slightly reoptimized taking into account the empirically determined tapering of the metal layers toward the embroidered walls.

E. Body Effects

To evaluate the effect of the human body, the antenna was simulated on top of a simplified three-layer human tissue model comprising skin, fat, and muscle as typically found in the literature [12]. As the antenna will rest on clothing that separates the antenna from body tissue, simulations were performed using 1- and 10-mm spacers to separate the antenna from the body tissue. This accounts for the varying space between the antenna and body tissue in practical situations.

The simulated free-space and on-body reflection coefficients are shown in Fig. 3(a), where it is observed that there is a frequency drift of 1.6% and a reduction in bandwidth from 3.8% to 3.0% for the on-body to free-space case. Current distribution plots (not shown for space constraints) reveal that there are significant currents on the side cavity walls as can be expected due to the nature of the slot. In the presence of dielectric loading, the current distribution is naturally varied, explaining the change in frequency and bandwidth. Considering now the effect of spacing Fig. 3(b), it is observed that there is a very mild drift over a range of expected spacing from the body, which is to be expected as the side currents are no longer in close proximity to

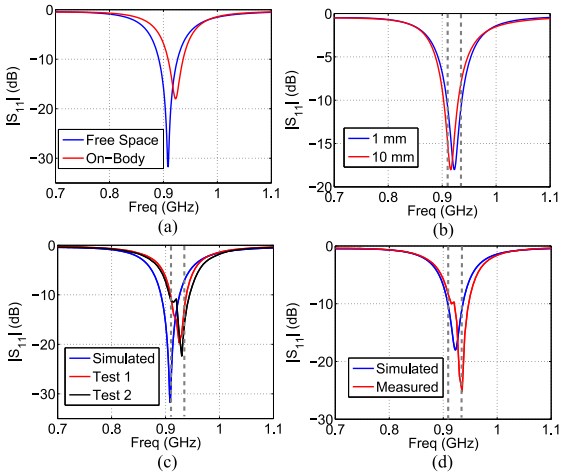

Fig. 3. (a) Simulated reflection coefficient in free space and on-body, (b) simulated reflection coefficient on-body with 1- and 10-mm spacing, (c) simulated and measured free-space reflection coefficient, and (d) simulated and measured on-body reflection coefficient.

a dielectric load. We address this issue through further isolation using a partial ground plane along the open aperture [13]—with dimension G_{EXT} shown in Fig. 1(a). This has the additional benefit of reducing energy absorption into lossy body tissue. If further isolation is required, then the ground plane can be made larger without adversely affecting wearability [5]. At this stage, the antenna reaches its final optimized dimensions of $0.34\lambda_0 \times 0.22\lambda_0 \times 0.0149\lambda_0$.

IV. Measurements

A. Fabrication

The fabrication procedure is as follows:

1) Cut 1.6- and 3.2-mm pieces of PF-4 foam to size.
2) Bond Marktex NCS95R-CR fabric to both sides of the 1.6-mm-thick piece and on one side of the 3.2-mm-thick piece.
3) Use a laser milling machine to pattern H-shaped slot and middle layer on opposite sides of the thinner piece and an SMA connector hole on both pieces of fabric.
4) Bond both pieces of foam together and perform computerized embroidery using Elitex Skin Contact 235 conductive threads with a linear stitching density of 1 mm five times over to realize cavity walls.
5) Extend an SMA jack connector with a protruding inner pin from bottom ground plane to top ground plane.
6) Apply conductive epoxy between center stripline and SMA inner pin.

B. Reflection Coefficient

To evaluate the performance of the antenna, reflection coefficient measurements were taken in free space and on-body. Free-space results are shown in Fig. 3(c) with two measurements (Test 1 and Test 2) provided. Both measurements show a similar resonance frequency, while Test 2 shows a mild notch. It is inferred then that the notch is not a feature of the antenna, but arises in difficulties in ensuring repeatable testing conditions (i.e., antenna flatness and mechanical strain). Additionally, a mild frequency drift is noted that is attributed to fabrication tolerances. As the antenna has been fabricated using a laser milling machine, the dimensions such as slot width, slot length, and gap

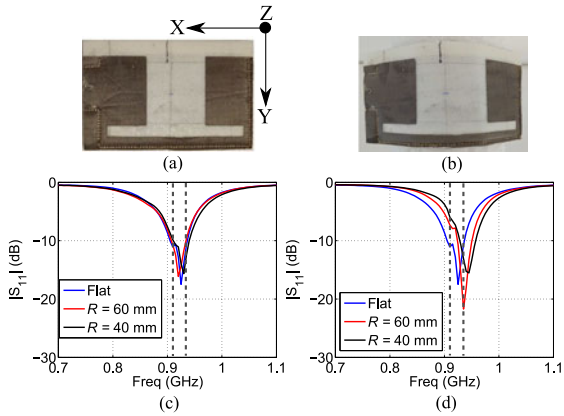

Fig. 4. (a) Antenna in flat state, (b) antenna bent along y-axis, (c) measured bending reflection coefficient in zy plane, and (d) measured bending reflection coefficient in zx plane.

size are expected to be very accurate. The variations in reflection coefficient are rather due to the mild reduction in the cavity size given the finite thickness of the embroidery walls, and to the light deviation from planar geometry for this flexible antenna.

On-body results are provided in Fig. 3(d) where good agreement between simulations and measurements is observed. At the lower end of the bandwidth, the measured reflection coefficient is approx -9.0 dB, which is acceptable for most wearable applications. Despite having a discrepancy in the free-space measurements, the on-body measurements are well correlated (with a measured frequency drift of 0.5%), which is attributed to the difficulty in knowing the exact dielectric constant of the body [14].

Overall, measured results show that the antenna largely satisfies the design specifications. Conditions such as bending and variations in spacing can lead to a mild degradation with measured worst case reflection coefficients rising to -6.0 dB at the margins of the targeted band of operation.

C. Bending Test

To characterize the effects of bending on performance, the antenna was bent along the zx, as shown in Fig. 4(a), and zy planes, as shown in Fig. 4(b), and the measured results are shown in Fig. 4(c) and (d) using typical bending radii of 40 and 60 mm [12]. It is observed that along the zy plane (left) there is little variability. The zx plane (right) shows more pronounced changes with worst case reflection at the sides of the band reaching -6.0 dB, which is to be expected given the significant currents along the H-shaped arm in this direction. Therefore, it is suggested: 1) bending with a small radius of curvature along the zx plane should be avoided; and 2) the antenna be placed on shoulder or torso regions where there is good mechanical support [1].

D. Radiation Patterns

The simulated and measured results for the H-plane (zy) and E-plane (zx) are given in Fig. 5 (top row) where generally good agreement is observed. Discrepancies are noted for the radiation patterns off broadside, which are attributed to the effect of the measurement setup (i.e., cables act as scatterers off broadside that are difficult to remove from measurements, and measurements are performed below the theoretical low-frequency limit of our anechoic chamber). In the zy plane, the simulated cross polarization is below -40 dB and not visible on the chosen

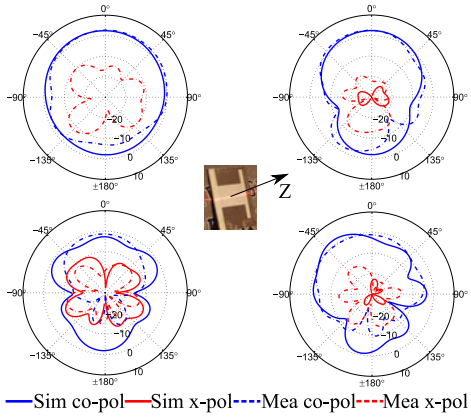

Fig. 5. Simulated and measured realized gain (dBi) patterns for free space (top row) and on-body (bottom row). Left column is *zy* plane and right column is *zx* plane.

TABLE I
LITERATURE COMPARISON

Ref.	Size (λ_0)	Thickness (λ_0)	BW (%)	Freq. (MHz)	ϵ_r	Eff. (%)
[5] (Wearable)	0.26	0.0098	0.70	923	1.06	60
[16] (PCB)	0.17	0.0016	–	870	2.08	–
[17] (PCB)	0.14	0.009	0.40	866	3.0	66
[18] (PCB)	0.41	0.0047	8.90	900	2.2	–
[15] (Wearable)	1.07	0.0322	6.70	2450	1.575	62
This work	0.34	0.0149	3.0	923	1.06	78

scale. The measured cross polarization of approx. -16 dB in both planes is generally higher than in simulations, and this is attributed to the imperfections and flexibility of the antenna, as well as the anechoic chamber being operated beyond the margins of its capability. Simulation results reveal a broadside gain of 2.4 dB, whilst the measured broadside gain is 2.6 dB. The simulated radiation efficiency is 78% and the good agreement with measured gain patterns suggests that the efficiency attained with our manufactured device should be very similar.

The radiation patterns were measured on a human body phantom (TORSO-OTA-V5.1) and are shown in Fig. 5 (bottom row). There is a discrepancy between simulations and measurements that is attributed to antenna tilting on the phantom (inset Fig. 5). Considering these factors, the simulated broadside gain is -2.7 dB with an off-broadside peak gain of 1.9 dB noted in the *zx* plane. A peak broadside gain of -1.3 dB is measured.

V. LITERATURE COMPARISON

Table I shows a comparison of the proposed geometry with other UHF antennas in the literature along with their largest dimension. While our antenna is slightly larger than some of the other antennas, this is compensated for by an increased bandwidth when placed in the vicinity of body tissue. Except for [5] and [15], none of the compared studies presents a textile realization. Noteworthy is the comparison of the current antenna to that of a cavity-backed slot antenna operating at 2.45 GHz where it is clearly seen that the antenna is more than double the relative thickness of the current antenna when scaling for the significantly higher frequency. This exemplifies the merits of the current design; if the current geometry was directly scaled to operate at 2.45 GHz, the obtained bandwidth would be larger than 6.70%.

VI. CONCLUSION

A miniaturized wearable cavity-backed slot-monopole antenna is proposed with a systematic design procedure. The major focus was the textile implementation of multiple miniaturization techniques able to generate a compact and efficient UHF radiating element. The antenna was shown to be easily integrable with a textile feeding mechanism. Dielectric loading was investigated where it was shown that the antenna can be made robust by a small ground plane extension, with a mild tradeoff in terms of size. The antenna is tolerant to mechanical deformations. A simple manufacturing process exploiting the use of a computerized embroidery machine enables an accurate realization. Good agreement between simulations and measurements implies that the proposed geometry is suitable for wearable applications.

REFERENCES

[1] P. Nepa and H. Rogier, "Wearable antennas for off-body radio links at VHF and UHF bands: Challenges, the state of the art, and future trends below 1 GHz," *IEEE Antennas Propag. Mag.*, vol. 57, no. 5, pp. 30–52, Oct. 2015.

[2] S. Shao, A. Kiourti, R. Burkholder, and J. Volakis, "Broadband textile-based passive UHF RFID tag antenna for elastic material," *IEEE Antennas Wireless Propag. Lett.*, vol. 14, pp. 1385–1388, 2015.

[3] S. Pinapati, T. Kaufmann, D. Ranasinghe, and C. Fumeaux, "Wearable dual-band stripline-fed half-mode substrate-integrated cavity antenna," *Electron. Lett.*, vol. 52, no. 6, pp. 424–426, Mar. 2016.

[4] K. Koski, L. Sydänheimo, Y. Rahmat-Samii, and L. Ukkonen, "Fundamental characteristics of electro-textiles in wearable UHF RFID patch antennas for body-centric sensing systems," *IEEE Trans. Antennas Propag.*, vol. 62, no. 12, pp. 6454–6462, Dec. 2014.

[5] T. Kaufmann, D. C. Ranasinghe, M. Zhou, and C. Fumeaux, "Wearable quarter-wave folded microstrip antenna for passive UHF RFID applications," *Int. J. Antennas Propag.*, vol. 2013, May, Art. no. 129839.

[6] S. Agneessens and H. Rogier, "Compact half diamond dual-band textile HMSIW on-body antenna," *IEEE Trans. Antennas Propag*, vol. 62, no. 5, pp. 2374–2381, May 2014.

[7] S. Jeon, Y. Yu, and J. Choi, "Dual-band slot-coupled dipole antenna for 900 MHz and 2.45 GHz RFID tag application," *Electron. Lett.*, vol. 42, no. 22, pp. 1259–1260, Oct. 2006.

[8] A. Wickramasinghe, D. C. Ranasinghe, C. Fumeaux, K. D. Hill, and R. Visvanathan, "Sequence learning with passive RFID sensors for real time bed-egress recognition in older people," *IEEE J. Biomed. Health Inform.*, vol. 21, no. 4, pp. 917–929, Jul. 2017.

[9] F. X. Liu, Z. Xu, D. C. Ranasinghe, and C. Fumeaux, "Textile folded half-mode substrate-integrated cavity antenna," *IEEE Antennas Wireless Propag. Lett.*, vol. 15, pp. 1693–1697, 2016.

[10] R. Moro, S. Agneessens, H. Rogier, A. Dierck, and M. Bozzi, "Textile microwave components in substrate integrated waveguide technology," *IEEE Trans. Microw. Theory Techn.*, vol. 63, no. 2, pp. 422–432, Feb. 2015.

[11] H. Li, J. Xiong, Y. Yu, and S. He, "A simple compact reconfigurable slot antenna with a very wide tuning range," *IEEE Trans. Antennas Propag.*, vol. 58, no. 11, pp. 3725–3728, Nov. 2010.

[12] S. Yan and G. Vandenbosch, "Radiation pattern-reconfigurable wearable antenna based on metamaterial structure," *IEEE Antennas Wireless Propag. Lett.*, vol. 15, pp. 1715–1718, 2016.

[13] G. A. Casula, A. Michel, P. Nepa, G. Montisci, and G. Mazzarella, "Robustness of wearable UHF-band PIFAs to human-body proximity," *IEEE Trans. Antennas Propag*, vol. 64, no. 5, pp. 2050–2055, May 2016.

[14] S. Gabriel, R. Lau, and C. Gabriel, "The dielectric properties of biological tissues: II. Measurements in the frequency range 10 Hz to 20 GHz," *Phys. Med. Biol.*, vol. 41, no. 11, p. 2251, 1996.

[15] R. Moro, S. Agneessens, H. Rogier, and M. Bozzi, "Wearable textile antenna in substrate integrated waveguide technology," *Electron. Lett.*, vol. 48, no. 16, pp. 985–987, 2012.

[16] C. Occhiuzzi, S. Cippitelli, and G. Marrocco, "Modeling, design and experimentation of wearable RFID sensor tag," *IEEE Trans. Antennas Propag.*, vol. 58, no. 8, pp. 2490–2498, Aug. 2010.

[17] M. Svanda and M. Polivka, "Small-size wearable high-efficiency TAG antenna for UHF RFID of people," *Int. J. Antennas Propag.*, vol. 2014, Mar. 2014, Art. no. 509768.

[18] A. Santiago, J. Costa, and C. Fernandes, "Broadband UHF RFID passive tag antenna for near-body applications," *IEEE Antennas Wireless Propag. Lett.*, vol. 12, pp. 136–139, 2013.